

Statistics of Scalar Flux Transport of Major Species in Different Premixed Turbulent Combustion Regimes for H_2 -air Flames

V. Papapostolou¹ · N. Chakraborty¹ · M. Klein² · H. G. Im³

Received: 7 May 2018 / Accepted: 20 September 2018 / Published online: 19 February 2019
© The Author(s) 2019

Abstract

The statistical behaviour of turbulent scalar flux and modelling of its transport have been analysed for both major reactants and products in the context of Reynolds Averaged Navier Stokes simulations using a detailed chemistry Direct Numerical Simulation (DNS) database of freely-propagating H_2 -air flames (with an equivalence ratio of 0.7) spanning the corrugated flamelets, thin reaction zones and broken reaction zones regimes of premixed turbulent combustion. The turbulent scalar flux in the cases representing the corrugated flamelets and thin reaction zones regimes of combustion exhibit predominantly counter-gradient transport, whilst a gradient transport has been observed for the broken reaction zones regime flame considered here. It has been found that the qualitative behaviour of the various terms of the turbulent scalar flux transport equation for the major species such as H_2 , O_2 and H_2O in the cases representing the corrugated flamelets and thin reaction zones regimes of combustion are mostly similar, whilst the behaviour is markedly different for the case representing the broken reaction zone regime. However, the terms for the scalar flux transport equation for H_2 and O_2 show same signs whereas the corresponding terms for H_2O show signs opposite to those for H_2 and O_2 . The performances of the well-established existing models for the unclosed terms of the turbulent scalar flux transport equation have been found to be similar for H_2 , O_2 and H_2O . Some of the existing models for turbulent flux, pressure gradient, molecular diffusion and reaction contributions have been found to yield reasonable performance for the cases representing the corrugated flamelets and thin reaction zones regimes but the existing closures for these terms have been found to be mostly inadequate for the broken reaction zones regime flames.

Keywords Turbulent scalar flux · Reynolds averaged Navier Stokes simulations · Direct numerical simulations · Premixed combustion · Counter-gradient transport

✉ N. Chakraborty
nilanjan.chakraborty@newcastle.ac.uk

1 Introduction

One of the major challenges of turbulent scalar transport modelling in the context of Reynolds Averaged Navier Stokes (RANS) simulations involves the closure of turbulent scalar flux components. The most widely used closure of turbulent scalar flux assumes a gradient hypothesis. According to the gradient hypothesis, the turbulent scalar flux components $\overline{\rho u_i'' Y_\alpha''}$ for compressible turbulent flows are modelled as [1]:

$$\overline{\rho u_i'' Y_\alpha''} = - \frac{\mu_t}{Sc_t} \frac{\partial \tilde{Y}_\alpha}{\partial x_i} \quad (1)$$

where ρ is the fluid density, u_i is the i^{th} component of fluid velocity, Y_α is the scalar in question (here Y_α is taken to be the mass fraction of species α), μ_t is the eddy viscosity, $Sc_t = \mu_t / \overline{\rho} D_t$ is the turbulent Schmidt number with D_t being the eddy diffusivity and $\tilde{q} = \overline{\rho q} / \overline{\rho}$ and $q'' = q - \tilde{q}$ are the Favre mean and fluctuations of a general variable q with the overline referring to the Reynolds averaging operation. The closure of $\overline{\rho u_i'' Y_\alpha''}$ using the gradient hypothesis has well-known limitations [2–8]. For example, $\overline{\rho u_i'' Y_\alpha''}$ and $(-\partial \tilde{Y}_\alpha / \partial x_i)$ are not collinearly aligned in turbulent channel flows. The difficulty in the modelling of $\overline{\rho u_i'' Y_\alpha''}$ is further exacerbated by the fact that the turbulent scalar flux shows a counter-gradient behaviour in turbulent premixed flames when the flame normal acceleration dominates over turbulent fluctuation [9–30]. Due to the limitation of algebraic closures of $\overline{\rho u_i'' Y_\alpha''}$, it is often necessary to solve a modelled transport equation of turbulent scalar flux components $\overline{\rho u_i'' Y_\alpha''}$ in the context of second-moment closure and probability density function based modelling methodologies [31–33].

Several analyses concentrated on the closures of turbulent fluxes of $\overline{\rho u_i'' Y_\alpha''}$ [34] and pressure gradient contributions [35–37] to the turbulent scalar flux transport for passive scalar mixing in non-reacting flows. However, the physics of turbulent scalar flux transport is considerably different in turbulent premixed flames due to the heat release arising from chemical reaction and self-induced pressure gradients. The modelling of the unclosed terms of the transport equation of $\overline{\rho u_i'' Y_\alpha''}$ for turbulent premixed flames was discussed by Bray et al. [9] for the flamelet regime of combustion, and the modelled transport equation of turbulent scalar flux was used by Lindstedt and Vaos [31] and Tian and Lindstedt [32] in RANS simulations of laboratory scale burners. The models for the unclosed terms have been assessed based on *a-priori* Direct Numerical Simulation (DNS) analysis by Nishiki et al. [20] for flames representing the corrugated flamelets regime [38]. Chakraborty and Cant [23–25] demonstrated that the characteristic Lewis number has a significant influence on the statistical behaviours of the unclosed terms of the turbulent scalar flux transport equation based on *a-priori* DNS analyses. Furthermore, the analysis of Chakraborty and Cant [24] proposed modifications to the existing model expressions for the unclosed terms of the turbulent scalar flux transport equation for non-unity Lewis number and also for the thin reaction zones [37] combustion regime. In a subsequent analysis [27] the same authors addressed the effects of turbulent Reynolds number on the closures of the various terms of the turbulent scalar flux transport equation. Recently, Lai et al. [39] also analysed the near-wall behaviours of the unclosed terms of the turbulent scalar flux transport equation based on DNS data of head-on quenching of statistically planar turbulent premixed flames with different turbulence intensities and characteristic Lewis numbers. Based on this analysis Lai et al. [39] proposed near-wall modifications to the models of the unclosed terms of the turbulent scalar flux transport equation. In this regard, it is worthwhile to mention that the

usage of turbulent scalar flux transport equation is rare in LES, whereas the turbulent scalar flux transport equation is used in the probability density function (PDF) method coupled with second-moment closure [31, 32]. Thus, an analysis of the turbulent scalar flux transport in the context of Large Eddy Simulations (LES) will be of limited relevance. As a result, this analysis focuses primarily on RANS modelling.

To date, all the analyses [9–30, 39] on the turbulent scalar flux transport in pre-mixed combustion modelling have been carried out in the context of simple chemistry and transport. With the advancement of high-performance computing, it is now possible to incorporate detailed chemical mechanisms and solve transport equations for several species in engineering simulations [40, 41]. It is not possible to translate the results for the turbulent scalar flux for one major species to any other major species by a linear transformation. The spatial distributions of each major species are different and thus the correlations between velocity and scalar fluctuations are different for every major species. For this reason, it is necessary to analyse the turbulent scalar fluxes for different major species in the context of multi-species RANS simulations. Moreover, it is necessary to ascertain if the same models for the unclosed terms in the transport equation of $\overline{\rho u_i'' Y_\alpha''}$ work equally well for all the major species α in different regimes of combustion. The present analysis addresses this gap in the existing literature by the analysis of turbulent scalar fluxes $\overline{\rho u_i'' Y_\alpha''}$ of H_2 , O_2 and H_2O , and the well-established sub-models of the transport equation of $\overline{\rho u_i'' Y_\alpha''}$ in the context of RANS using a three-dimensional Direct Numerical Simulations (DNS) database of H_2 -air flames with an equivalence ratio of 0.7 (which ensures that the flames remain globally thermo-diffusively neutral with respect to flame speed response to flame stretch [42]). The simulation parameters for this DNS database have been chosen in such a manner that the cases considered here represent typical combustion situations within the corrugated flamelets, thin reaction zones and broken reaction zones regimes of premixed turbulent combustion. The turbulent scalar fluxes $\overline{\rho u_i'' Y_\alpha''}$ of H_2 , O_2 and H_2O , and the transport equation of these scalar fluxes have been analysed using the aforementioned DNS database. Moreover, the modelling of the unclosed terms of the turbulent scalar flux transport equations will be discussed for the mass fractions of H_2 , O_2 and H_2O .¹ In this respect, the main objectives of this paper are:

- To analyse the statistical behaviours of turbulent scalar fluxes $\overline{\rho u_i'' Y_\alpha''}$ for H_2 , O_2 and H_2O mass fractions (i.e. $\alpha = H_2$, O_2 and H_2O) and the unclosed terms of the transport equation of $\overline{\rho u_i'' Y_\alpha''}$ in different regimes of combustion.
- To provide physical explanations for the differences in the behaviour of turbulent scalar fluxes $\overline{\rho u_i'' Y_\alpha''}$ for different major species in different combustion regimes.
- To assess the performances of the models for the unclosed terms of the transport equation of $\overline{\rho u_i'' Y_\alpha''}$ for $\alpha = H_2$, O_2 and H_2O in different combustion regimes.

The modelling attempts for the turbulent scalar flux transport in the context of turbulent reacting flows are relatively scarce [9, 20, 24, 27, 39] and all the existing analyses on turbulent premixed flames have been carried out for the flames in the flamelets regime using simple chemical mechanism [9, 20]. Until now no model has been proposed for the low-Damköhler number conditions in the broken reaction zones regime. In this paper, the

¹The turbulent scalar fluxes of sensible enthalpy and temperature (i.e. $\overline{\rho u_i'' h''}$ and $\overline{\rho u_i'' T''}$) exhibit similar qualitative behaviour as that of $\overline{\rho u_i'' Y_{H_2O}''}$ and thus are not explicitly discussed for the purpose of conciseness.

turbulent scalar flux transport has been addressed in the context of detailed chemical mechanism and non-unity Lewis number for the very first time. It is not to be expected that this analysis will provide solutions to the modelling challenges that are open in the literature for decades and therefore the current paper should be treated as a first step towards achieving the goal of having a unified model of turbulent scalar flux transport for all regimes of premixed combustion for a multi-species system.

The rest of the paper will be organised as follows. The mathematical background and numerical implementation pertaining to the current analysis are provided in the next two sections. Following that, results are presented and discussed. The main findings are summarised and conclusions are drawn in the final section of this paper.

2 Mathematical Background

The transport equation of the Favre-averaged mass fraction $\tilde{Y}_\alpha = \overline{\rho Y_\alpha} / \bar{\rho}$ of species α is given by:

$$\partial(\bar{\rho}\tilde{Y}_\alpha)/\partial t + \partial(\bar{\rho}\tilde{u}_j\tilde{Y}_\alpha)/\partial x_j = \overline{\dot{\omega}_{Y_\alpha}} + \partial[\overline{\rho D_\alpha(\partial Y_\alpha/\partial x_j)}]/\partial x_j - \partial(\overline{\rho u_j'' Y_\alpha''})/\partial x_j \quad (2)$$

where $\dot{\omega}_Y$ and D_α are the chemical reaction rate of species α and diffusivity of species α , respectively. The last term on the right-hand side of Eq. 2 indicates turbulent transport of species α and one requires a model for the turbulent scalar flux $\overline{\rho u_j'' Y_\alpha''}$. Using the transport equations of Y_α and u_i , it is possible to derive a transport equation for $\overline{\rho u_i'' Y_\alpha''}$, which takes the following form [9, 20, 23–25, 39]:

$$\begin{aligned} \frac{\partial \overline{\rho u_i'' Y_\alpha''}}{\partial t} + \frac{\partial \tilde{u}_j \overline{\rho u_i'' Y_\alpha''}}{\partial x_j} = & \underbrace{-\frac{\partial \overline{\rho u_j'' u_i'' Y_\alpha''}}{\partial x_j}}_{T_1} - \underbrace{\overline{\rho u_i'' u_j''}}_{T_2} \frac{\partial \tilde{Y}_\alpha}{\partial x_j} \\ & - \underbrace{\overline{\rho u_j'' Y_\alpha''}}_{T_3} \frac{\partial \tilde{u}_i}{\partial x_j} - \underbrace{\overline{Y_\alpha''}}_{T_4} \frac{\partial \bar{P}}{\partial x_i} - \underbrace{\overline{Y_\alpha''}}_{T_5} \frac{\partial \bar{P}'}{\partial x_i} + \underbrace{[\overline{u_i''} \frac{\partial}{\partial x_k} (\rho D \frac{\partial Y_\alpha}{\partial x_k})]}_{T_6} + \underbrace{[\overline{Y_\alpha''} \frac{\partial \tau_{ik}}{\partial x_k}]}_{T_7} + \underbrace{\overline{u_i'' \dot{\omega}_{Y_\alpha}}}_{T_8} \end{aligned} \quad (3)$$

where $\tau_{ij} = \mu[(\partial u_i/\partial x_j) + (\partial u_j/\partial x_i)] - (2\mu/3)\delta_{ij}(\partial u_k/\partial x_k)$ is the viscous stress tensor, P is the pressure and μ is the dynamic viscosity. The term T_1 is associated with turbulent transport of $\overline{\rho u_i'' Y_\alpha''}$, whereas T_2 and T_3 represent generation of turbulent scalar flux $\overline{\rho u_i'' Y_\alpha''}$ by mean species and velocity gradients respectively. The terms T_4 and T_5 denote the contributions of mean and fluctuating pressure gradients respectively. The combined contributions of T_6 and T_7 is referred to as the molecular diffusion term. The term T_8 is the chemical reaction rate contribution to the turbulent scalar flux $\overline{\rho u_i'' Y_\alpha''}$ transport. The statistical behaviours of $T_1 - T_8$ and their modelling will be discussed for turbulent scalar flux transports of H_2 , O_2 and H_2O in Section 4 of this paper.

3 Numerical Implementation

In order to analyse the statistical behaviours of $\overline{\rho u_i'' Y_\alpha''}$, and $T_1 - T_8$ a three-dimensional detailed chemistry (9 species and 19 chemical reactions) DNS database of statistically

planar H_2 -air flames with an equivalence ratio of 0.7 (i.e. $\phi = 0.7$) was used [43]. The simulations have been conducted using a well-known DNS code [43], which employs high-order finite differences (8th order at the internal grid points and gradually reducing to a one-sided 4th order scheme at the non-periodic boundary) and a high order Runge-Kutta (4th order) scheme for spatial discretisation and explicit time advancement respectively. The reacting scalar field has been initialised using the steady laminar H_2 -air flame solution corresponding to $\phi = 0.7$. The thermo-physical properties are taken to be temperature dependent and are expressed according to CHEMKIN polynomials. The unburned gas temperature T_0 is taken to be 300K, which leads to an unstrained laminar burning velocity $S_L = 135.6\text{cm/s}$ and heat release parameter $\tau = (T_{ad} - T_0)/T_0 = 5.71$ (where T_{ad} is the adiabatic flame temperature) under atmospheric pressure. The numerical implementation for this database has been discussed elsewhere [43] in detail and thus a brief description is provided here. Turbulent inflow and outflow boundaries are taken in the direction of mean flame propagation, and transverse boundaries are considered to be periodic. The inflow and outflow boundaries are specified using an improved Navier Stokes characteristic boundary conditions (NSCBC) technique [44]. The inflow turbulent velocity fluctuations are specified by scanning a plane through a frozen field of turbulent homogeneous incompressible velocity generated using a pseudo-spectral method [45] following the Passot-Pouquet spectrum [46]. The inflow values of normalised root-mean-square turbulent velocity fluctuation u'/S_L , turbulent length scale to flame thickness ratio l_T/δ_{th} , flame thickness to the Kolmogorov length scale ratio δ_{th}/η Damköhler number $Da = l_T S_L/u'\delta_{th}$, Karlovitz number $Ka = (\rho_0 S_L \delta_{th}/\mu_0)^{0.5} (u'/S_L)^{1.5} (l_T/\delta_{th})^{-0.5}$ and turbulent Reynolds number $Re_t = \rho_0 u' l_T/\mu_0$ for all cases are presented in Table 1 where ρ_0 and μ_0 are the unburned gas density and viscosity, respectively, $\delta_{th} = (T_{ad} - T_0)/\max|\nabla T|_L$ is the thermal flame thickness (with 'L' denoting unstrained laminar flame quantities). Cases A–C are representative of the corrugated flamelets ($Ka < 1$), thin reaction zones ($1 < Ka < 100$) and broken reaction zones ($Ka > 100$) regimes [38] of premixed turbulent combustion respectively. The domain size is $20\text{mm} \times 10\text{mm} \times 10\text{mm}$ ($8\text{mm} \times 2\text{mm} \times 2\text{mm}$) in cases A and B (case C) and the domain has been discretised by a uniform mesh of dimension $512 \times 256 \times 256$ ($1280 \times 320 \times 320$). The mean inlet velocity has been adjusted to match the turbulent flame speed and the temporal evolution of the flame area has been monitored until a quasi-steady state is reached. The statistical stationary state has been achieved at a time corresponding to $1.0l_T/u'$, $6.8l_T/u'$, $6.7l_T/u'$ for cases A–C respectively and this simulation time remains comparable to several previous analyses [47–49]. For statistically planar flames, the directions normal to the mean direction of flame propagation (i.e. x_1 -direction) are statistically homogeneous. All the Reynolds/Favre averaging operations have been conducted by ensemble averaging the variables in the directions normal to the mean direction of flame propagation.

Table 1 List of inflow turbulence parameters

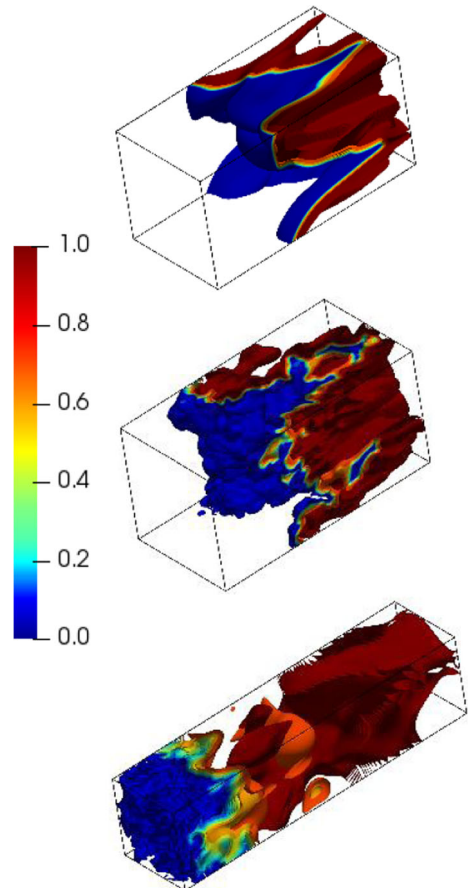
Case	u'/S_L	l_T/δ_{th}	δ_{th}/η	Re_t	Da	Ka
A	0.7	14.0	4.17	227	20.0	0.75
B	5	14.0	18.26	1623	2.8	14.4
C	14	4.0	53.91	1298	0.29	126

4 Results & Discussion

4.1 Flame-turbulence interaction

The isosurfaces of non-dimensional temperature $c_T = (T - T_0)/(T_{ad} - T_0)$ for cases A-C are shown in Fig. 1, which indicates that the flame morphologies in these cases are significantly different from each other and interested readers are referred to Refs. [43, 50] for further discussion in this regard. The flame wrinkling can be quantified based on the normalised flame surface area A/A_0 where the flame surface area A is evaluated as: $A = \int_V |\nabla c| dV$ and A_0 is the initial value of flame surface area based on the one-dimensional steady state laminar flame solution. The quasi-steady state values of A/A_0 are 3.25, 5.0 and 3.25 for cases A, B and C respectively. The inlet turbulence intensity u'/S_L increases from case A to B, which leads to a greater extent of flame wrinkling in case B than in case A. However, l_T/δ_{th} values in cases A and C are considerably different and thus, the extent of flame wrinkling in cases A and C remain comparable despite large differences in u'/S_L values. It should be noted that Ka has not been modified here in isolation and thus the differences in behaviours of $T_1 - T_8$ originate not only due to the changes in the variation of Ka but also due to the changes in Da .

Fig. 1 Isosurfaces of c_T for Cases A-C (top to bottom) when the statistics were extracted



4.2 Statistical behaviour of turbulent scalar flux

In the case of statistically planar flames, $\overline{\rho u''_1 Y''_\alpha}$ is the only non-zero component of turbulent scalar flux. The variations of $\overline{\rho u''_1 Y''_\alpha} \times 1/\rho_0 S_L |Y_{\alpha u} - Y_{\alpha b}|$ (where subscripts u and b refer to the values in unburned and burned gases respectively and the multiplier is used for normalisation) with \tilde{c}_T are shown in Fig. 2. The signs of $\overline{\rho u''_1 Y''_\alpha}$ for $\alpha = H_2$ and O_2 are the same but are different to $\overline{\rho u''_1 Y''_\alpha}$ for $\alpha = H_2O$. Moreover, it can be seen from Fig. 2 that the qualitative behaviour of $\overline{\rho u''_1 Y''_\alpha}$ for $\alpha = H_2, O_2$ and H_2O does not change in cases A and B but the behaviour in case C is completely different from that in cases A and B. In order to understand this observation the variation of $\Lambda = \overline{\rho u''_1 Y''_\alpha} / (-\partial \tilde{Y}_\alpha / \partial x_1) \times 1/\rho_0 S_L \delta_{th}$ with \tilde{c}_T is shown for all cases in Fig. 3 for $\alpha = H_2, O_2$ and H_2O . A positive (negative) value of $\overline{\rho u''_1 Y''_\alpha} / (-\partial \tilde{Y}_\alpha / \partial x_1)$ is indicative of a gradient (counter-gradient) transport. Furthermore, for a gradient transport $\overline{\rho u''_1 Y''_\alpha} / (-\partial \tilde{Y}_\alpha / \partial x_1)$ provides the density-weighted eddy diffusivity $\overline{\rho} D_t$, whereas an unphysical negative $\overline{\rho} D_t$ is obtained for a counter-gradient transport. Figure 3 indicates that a predominantly counter-gradient behaviour has been observed for

Fig. 2 Variation of $\overline{\rho u''_1 Y''_\alpha} \times 1/\rho_0 S_L |Y_{\alpha u} - Y_{\alpha b}|$ with \tilde{c}_T for cases A–C (top to bottom) for $\alpha = H_2, O_2$ and H_2O

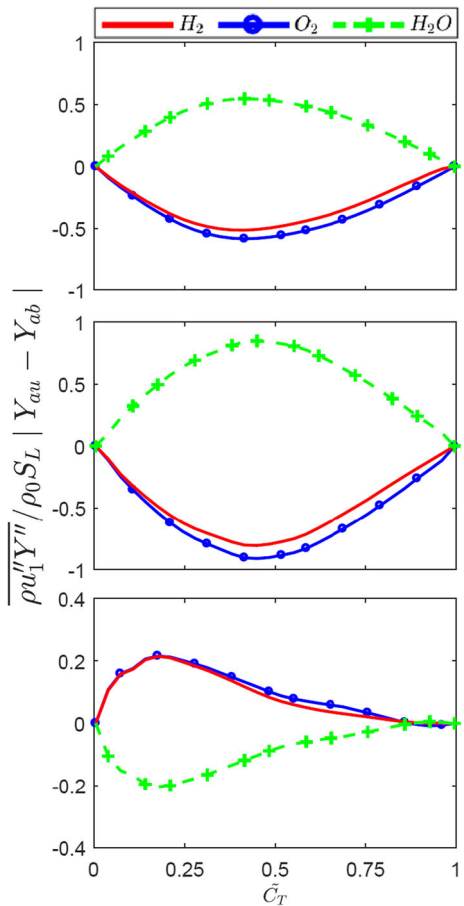
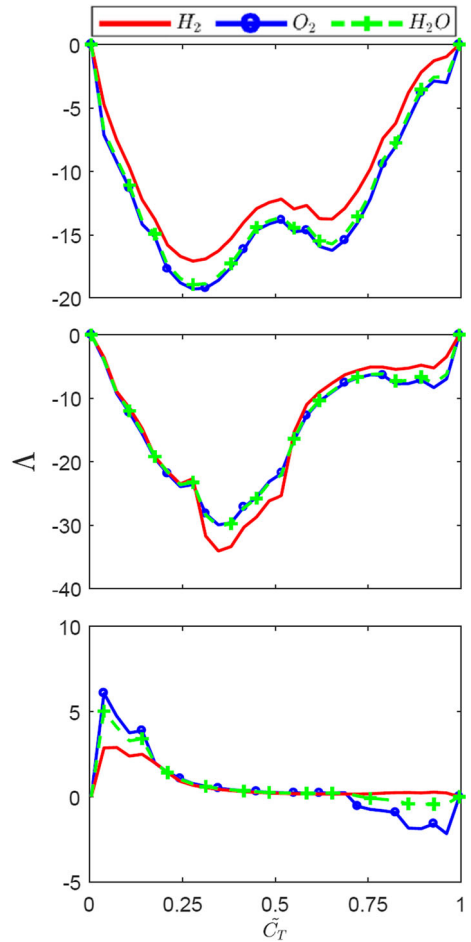


Fig. 3 Variation of $\Lambda = \rho u''_i Y''_\alpha / (-\partial \tilde{Y}_\alpha / \partial x_1) \times (1/\rho_0 S_L \delta_{th})$ with \tilde{c}_T for cases A-C (top to bottom) for $\alpha = H_2, O_2$ and H_2O



turbulent scalar fluxes of H_2, O_2 and H_2O for cases A and B, whereas a gradient type transport is obtained for these species in case C.

It is important to note that the results in Fig. 3 do not necessarily mean that counter-gradient (gradient) transport will always be obtained for the flames within the corrugated flamelets and thin reaction zones regimes (broken reaction zones regime). According to Veynante et al. [12], a gradient transport is obtained for $N_B < 1$, whereas a counter-gradient transport is favoured for $N_B > 1$, where $N_B = \tau S_L / 2\alpha u'$ is the Bray number with α being an efficiency function. The value of α is about 0.5 according to Veynante et al. [12] and thus $\tau S_L / u'$ can be taken to provide a measure of the Bray number N_B . The Bray number criterion proposed by Veynante et al. [12] is valid in an order of magnitude sense. The velocity jump due to flame normal acceleration arising from chemical heat release is taken to scale with τS_L , whereas the velocity jump due to turbulence scales with u' . A counter-gradient transport is obtained when τS_L dominates over u' , whereas a gradient transport is obtained when u' dominates over τS_L . In cases A and B, $\tau S_L / u'$ remains greater than unity (= 8.16 for case A and 1.14 for case B) whereas it is smaller than unity (= 0.41) for case C

and accordingly a counter-gradient behaviour has been observed for cases A and B whilst a gradient transport is obtained for case C.

4.3 Statistical behaviour of the terms of the turbulent scalar flux transport equation

The variations of $T_1 - T_8$ with \tilde{c}_T in cases A-C are shown in Fig. 4 for $\alpha = H_2, O_2$ and H_2O so that the relative magnitudes of these terms for different species can be compared for flames belonging to the different combustion regimes. The modelling of the terms of the turbulent scalar flux transport equation will be discussed in the subsequent sub-sections. The signs of these terms for H_2O are different from those of H_2 and O_2 for all cases because H_2O is a product species, whereas H_2 and O_2 are the reactants. It is worth noting that a positive (negative) contribution of $T_1 - T_8$ acts to produce a counter-gradient (gradient) transport of turbulent scalar flux $\overline{\rho u_1'' Y_{H_2O}''}$. By contrast, a negative (positive) value of $T_1 - T_8$ promotes a counter-gradient (gradient) transport of turbulent scalar fluxes of H_2 and O_2 (i.e. $\overline{\rho u_1'' Y_{H_2}''}$ and $\overline{\rho u_1'' Y_{O_2}''}$). The mean and fluctuating pressure gradient terms T_4 and T_5 play leading order roles in cases A and B. For case C, T_4 and T_5 remain comparable to the magnitudes of the contributions of T_1, T_2, T_6 and T_8 . The flame normal acceleration sets up a negative mean pressure gradient (i.e. $\partial \bar{P} / \partial x_1 < 0$ when the mean direction of flame propagation is in the negative x_1 -direction), which gives rise to negative (positive) values of T_4 for reactants (products) because of negative (positive) values of \bar{Y}_α'' . A negative (positive) fluctuation of Y_α'' for reactants (products) tends to induce a more negative pressure gradient and thus $T_5 = -\overline{Y_\alpha'' (\partial P' / \partial x_1)}$ assumes mostly positive (negative) values for $\alpha = H_2$ and O_2 ($\alpha = H_2O$). The terms due to mean species and velocity gradients T_2 and

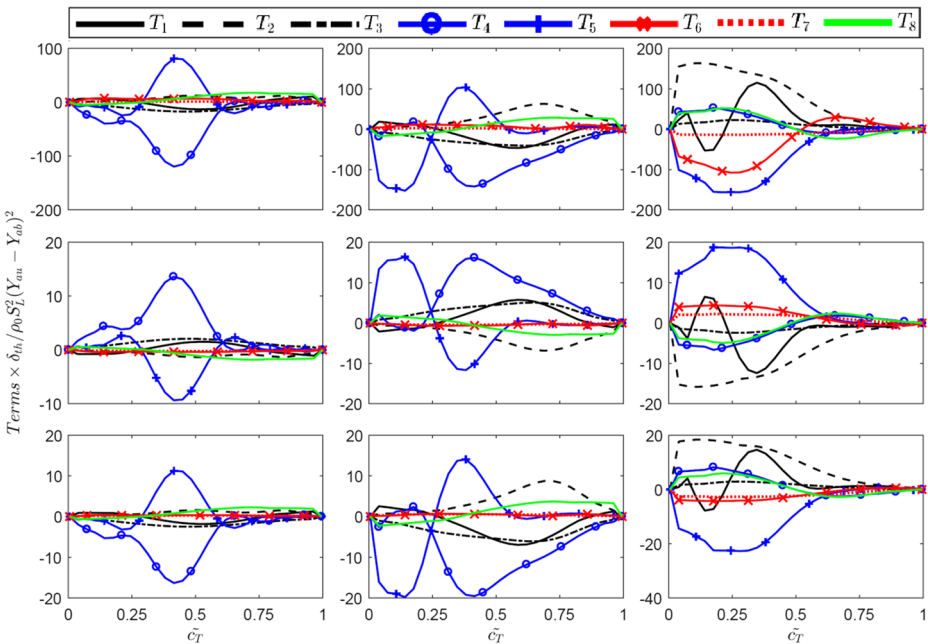


Fig. 4 Variations of $T_1 - T_8$ normalised by $\delta_{th} / \rho_0 S_L^2 (Y_{\alpha u} - Y_{ab})^2$ with \tilde{c}_T for the turbulent scalar flux transports of H_2, H_2O and O_2 (1st-3rd row) for cases A-C (1st-3rd column) for $\alpha = H_2, O_2$ and H_2O

T_3 exhibit positive (negative) values across the flame brush for H_2 and $O_2(H_2O)$ in cases A and B. In case C, T_2 assumes positive (negative) values across the flame brush for H_2 and $O_2(H_2O)$, whereas the magnitude of T_3 remains negligible in comparison to the contributions of T_1, T_2, T_4, T_5, T_6 and T_8 but this term assumes negative (positive) values within the flame brush for H_2 and $O_2(H_2O)$. For statistically planar flames with the mean direction of flame propagation aligned with x_1 -direction, the term $T_2 = -\overline{\rho u_1'' u_1'' (\partial \tilde{Y}_\alpha / \partial x_1)}$ assumes negative values for product species (e.g. H_2O) because $\partial \tilde{Y}_\alpha / \partial x_1$ and $\overline{\rho u_1'' u_1''}$ assume positive values. By contrast, positive values of T_2 are obtained for reactant species (e.g. H_2 and O_2) in statistically planar flames because of predominantly negative values of $\partial \tilde{Y}_\alpha / \partial x_1$. For statistically planar flames T_3 can be expressed as: $T_3 = -\overline{\rho u_1'' Y_\alpha'' (\partial \tilde{u}_1 / \partial x_1)}$ and thus the sign of T_3 depends on $\overline{\rho u_1'' Y_\alpha''}$ because $(\partial \tilde{u}_1 / \partial x_1)$ is expected to be positive due to flame normal acceleration as a result of heat release. In cases A and B, $\overline{\rho u_1'' Y_\alpha''}$ assumes negative (positive) values within the flame brush for reactants (products), which leads to positive (negative) values of T_3 for $\alpha = H_2$ and O_2 ($\alpha = H_2O$). By contrast, $\overline{\rho u_1'' Y_\alpha''}$ assumes positive (negative) values within the flame brush for reactants (products) in case C, which leads to negative (positive) values of T_3 for $\alpha = H_2$ and O_2 ($\alpha = H_2O$).

The molecular diffusion terms T_6 and T_7 play marginal roles in cases A and B but T_6 plays a leading order role in case C, especially for the turbulent scalar flux transport of H_2 . It can be seen from Fig. 4 that the combined action of T_6 and T_7 acts to reduce the extent of counter-gradient transport in cases A and B, whereas it acts to reduce the extent of gradient transport in case C, and this behaviour remains unchanged for all species considered here. The combined contribution of T_6 and T_7 can be split into a molecular diffusion contribution ($\propto \nabla \cdot (\rho D \nabla (u_1'' Y_\alpha''))$) and a dissipation contribution ($\propto -2\rho D \nabla Y_\alpha'' \cdot \nabla u_1''$). For high values of Re_t the molecular dissipation contribution dominates over the diffusion contribution (i.e. $|\nabla \cdot (\rho D \nabla (u_1'' Y_\alpha''))| \ll | -2\rho D \nabla Y_\alpha'' \cdot \nabla u_1'' |$). For a counter-gradient transport, the quantity $2\rho D \nabla Y_\alpha'' \cdot \nabla u_1''$ assumes positive (negative) values for products (reactants) and thus the contribution of $(T_6 + T_7)$ acts to reduce the extent of counter-gradient transport in cases A and B. By contrast, $2\rho D \nabla Y_\alpha'' \cdot \nabla u_1''$ assumes negative (positive) values for products (reactants) for a gradient transport, and thus it acts to reduce the extent of gradient transport in case C.

The reaction rate contribution T_8 assumes positive (negative) values towards the unburned gas side of the flame brush, before becoming negative (positive) on the burned gas side of the flame brush for H_2 and O_2 (H_2O) for all cases, but for cases A and B this term remains small in comparison to the magnitudes of T_4 and T_5 , whereas its magnitude is comparable to T_1, T_2, T_4, T_5 and T_6 in case C. An increase (decrease) in reaction rate magnitude on the unburned (burned) gas side tends to induce a negative u_1'' due to the decay of turbulence under the enhanced viscous action, and this leads to positive (negative) values towards the unburned gas side of the flame brush and negative (positive) values of T_8 on the burned gas side of the flame brush for reactants such as $\alpha = H_2$ and O_2 (for products such as $\alpha = H_2O$) for all cases. However, this action is relatively stronger in case C than in cases A and B because flame-generated turbulence effects are stronger in these cases. The flame-generated turbulence acts to locally enhance the turbulence level in cases A and B, which counters the decay of turbulence with increased chemical activity and thus the relative magnitude of T_8 is smaller than the leading order contributions of T_4 and T_5 in these cases in comparison to case C.

It is worth noting that the observed behaviours from Fig. 4 are consistent with the scaling analyses presented in Chakraborty and Cant [27] and Lai et al. [39], which indicate that T_2

and T_4 are expected to play dominant roles in the turbulent scalar flux transport and T_3 is likely to be of marginal importance for high Reynolds number flames with small values of Da (i.e. $Da < 1$).

The terms T_2 and T_3 are closed terms in the context of second-moment closure because $\overline{\rho u_i'' u_j''}$ and $\overline{\rho u_j'' Y_\alpha''}$ are already modelled in this framework. The terms T_1, T_4, T_5, T_6, T_7 and T_8 are unclosed and need closures in order to solve Eq. 2. This is often achieved by modelling $\overline{\rho u_j'' u_i'' Y_\alpha''}, (T_4 + T_5), (T_6 + T_7)$ and T_8 , which will be discussed next in this paper.

4.4 Modelling of turbulent flux of scalar flux $\overline{\rho u_j'' u_i'' Y_\alpha''}$

The quantity $\overline{\rho u_1'' u_1'' Y_\alpha''}$ is the only non-zero component of $\overline{\rho u_i'' u_i'' Y_\alpha''}$ for a statistically planar flame. The turbulent flux of $\overline{\rho u_i'' Y_\alpha''}$ is usually modelled for non-reacting flows in the following manner utilising the gradient hypothesis [34]:

$$\overline{\rho u_j'' u_i'' Y_\alpha''} = -C_{CS} \frac{\tilde{k}}{\tilde{\epsilon}} \overline{\rho u_j'' u_k''} \frac{\partial (\overline{\rho u_i'' Y_\alpha''} / \bar{\rho})}{\partial x_k} \tag{4}$$

This model will henceforth be referred to as the TDH (triple-correlation Daly-Harlow) model in this paper. Equation 4 is based on a gradient hypothesis and thus is incapable of addressing counter-gradient behaviour. Moreover, Eq. 4 does not account for flame normal acceleration effects arising from chemical heat release which are responsible for counter-gradient transport.

Subject to the assumption of a bimodal probability density function of c (i.e. $P(c)$ with impulses at $c=0$ and $c=1$) according to the Bray-Moss-Libby (BML) analysis, the Favre-average velocity component takes the following form: $\tilde{u}_j = \overline{(u_j)}_P \tilde{c} + (1-\tilde{c}) \overline{(u_j)}_R + O(1/Da)$, which upon using in $\overline{\rho u_i'' u_j'' c''} = \int_{-\infty}^{\infty} \int_{-\infty}^{\infty} \int_0^1 \rho(u_i - \tilde{u}_i)(u_j - \tilde{u}_j)(c - \tilde{c}) P(u_i; u_j; c) du_i du_j dc$ provides [27, 39]:

$$\overline{\rho u_1'' u_1'' c''} \approx \bar{\rho} \left[\overline{(u_1)}_P - \overline{(u_1)}_R \right]^2 \tilde{c}(1-\tilde{c})(1-2\tilde{c}) - \bar{\rho} \overline{(u_1' u_1')}_R \tilde{c}(1-\tilde{c}) + \bar{\rho} \overline{(u_1' u_1')}_P \tilde{c}(1-\tilde{c}) + O(1/Da) \tag{5i}$$

The first term on the right-hand side represents the reacting contribution to $\overline{\rho u_1'' u_1'' c''}$, whereas the combined action of second and third terms represent the effects of turbulence on $\overline{\rho u_1'' u_1'' c''}$. The last term $O(1/Da)$ originates from the interior of the flame, and this contribution becomes negligible for $Da \gg 1$. Chakraborty and Cant [24, 27] proposed an alternative model of $\overline{\rho u_1'' u_1'' Y_\alpha''}$ by incorporating the reacting contribution according to the Bray-Moss-Libby (BML) analysis and the turbulent contribution in Eq. 5i is accounted for by the TDH model. The model by Chakraborty and Cant [24, 27] is given by:

$$\begin{aligned} \overline{\rho u_1'' u_1'' Y_\alpha''} = & -C_{CS} \frac{\tilde{k}}{\tilde{\epsilon}} \overline{\rho u_1'' u_1''} \frac{\partial (\overline{\rho u_1'' Y_\alpha''} / \bar{\rho})}{\partial x_1} - \frac{\bar{\rho} (Y_{\alpha u} - \tilde{Y}_\alpha) (\tilde{Y}_\alpha - Y_{\alpha b})}{(Y_{\alpha u} - Y_{\alpha b})} \left[1 - 2\sqrt{g} \frac{Y_{\alpha u} - \tilde{Y}_\alpha}{(Y_{\alpha u} - Y_{\alpha b})} \right] \\ & \times \left[\frac{-\overline{\rho u_1'' Y_\alpha''} (Y_{\alpha u} - Y_{\alpha b})}{\bar{\rho} (Y_{\alpha u} - \tilde{Y}_\alpha) (\tilde{Y}_\alpha - Y_{\alpha b})} + a_3 \sqrt{\frac{\overline{\rho u_1'' u_1''}}{\bar{\rho}}} \right]^2 \text{ where } a_3 = 0.5; g = \frac{\overline{\rho Y_\alpha''^2}}{\bar{\rho} (Y_{\alpha u} - \tilde{Y}_\alpha) (\tilde{Y}_\alpha - Y_{\alpha b})} \end{aligned} \tag{5ii}$$

Equation 5ii will henceforth be referred to as the CC model in this paper. The second term on the right hand side of Eq. 5ii is capable of predicting counter-gradient transport and includes the effects of flame normal acceleration due to chemical heat release (i.e. $-\rho u_1'' Y_\alpha'' (Y_{\alpha u} - Y_{\alpha b}) / [\bar{\rho} (Y_{\alpha u} - \bar{Y}_\alpha) (\bar{Y}_\alpha - Y_{\alpha b})] + a_3 \sqrt{\rho u_1'' u_1'' / \bar{\rho}}$) in Eq. 5ii accounts for the velocity jump across the flame brush with the first term representing the effects of heat release, whereas the second term represents the effects of turbulent velocity fluctuations).

The predictions of the TDH and CC models are compared to $\overline{\rho u_1'' u_1'' Y_\alpha''}$ extracted from DNS data in Fig. 5 for $\alpha = H_2, O_2$ and H_2O . In cases A and B, $\overline{\rho u_1'' u_1'' Y_\alpha''}$ assumes negative (positive) values towards the unburned (burned) gas side of the flame brush for $\alpha = H_2$ and O_2 but just the opposite behaviour is obtained for $\alpha = H_2O$. In case C, $\overline{\rho u_1'' u_1'' Y_\alpha''}$ assumes predominantly positive values for $\alpha = H_2$ and O_2 , whereas predominantly negative values of $\overline{\rho u_1'' u_1'' Y_\alpha''}$ are obtained for $\alpha = H_2O$.

It can be seen from Fig. 5 that both TDH and CC models do not adequately predict $\overline{\rho u_1'' u_1'' Y_\alpha''}$ in case C for $\alpha = H_2, O_2$ and H_2O . The TDH model predicts an incorrect sign of $\overline{\rho u_1'' u_1'' Y_\alpha''}$ for cases A and B for $\alpha = H_2, O_2$ and H_2O , which implies that $\overline{\rho u_1'' u_1'' Y_\alpha''}$ exhibits counter-gradient behaviour in these cases. In cases A and B, the CC model has been found to accurately predict the quantitative behaviour of $\overline{\rho u_1'' u_1'' Y_{H_2}''}$ and $\overline{\rho u_1'' u_1'' Y_{O_2}''}$ on the unburned gas side of the flame brush, but does not predict the correct trend on the burned gas side of the flame brush and its prediction becomes comparable to the TDH model. This implies that the magnitude of the second term on the right hand side of Eq. 5i–5iii becomes

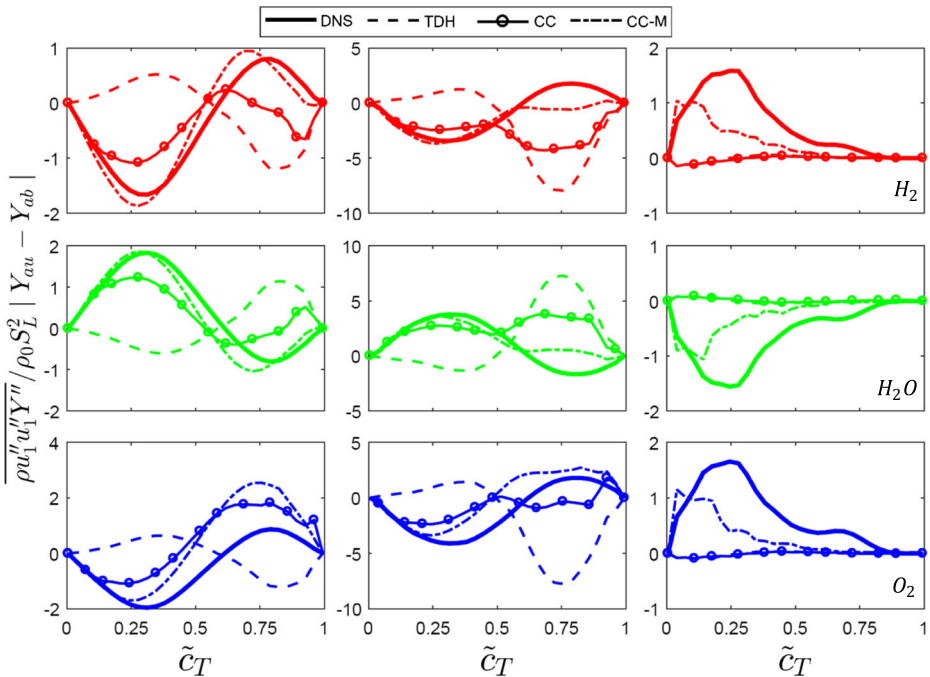


Fig. 5 Variation of $\overline{\rho u_1'' u_1'' Y_\alpha''} \times 1 / \rho_0 S_L^2 |Y_{\alpha u} - Y_{\alpha b}|$ with \tilde{c}_T across the flame brush along with the predictions of the TDH, CC and CC-M models for cases A-C (1st-3rd column) for $\alpha = H_2, O_2$ and H_2O

small in comparison to the first term towards the burned gas side of the flame brush for $\alpha = H_2$ and O_2 in cases A and B. The CC model captures the correct qualitative behaviour of $\overline{\rho u''_1 u''_1 Y''_{H_2O}}$ for case A and the quantitative agreement also remains reasonable. However, in case B the CC model predicts the qualitative and quantitative behaviours of $\overline{\rho u''_1 u''_1 Y''_{H_2O}}$ towards the leading edge and the middle of the flame brush and its prediction becomes qualitatively and quantitatively similar to the TDH model towards the burned gas side. The predictions of the CC model can be improved further by modifying the model parameters C_{Cs} and a_3 and the optimum values of these parameters for cases A-C are listed in Table 2. These optimum values have been parameterised for $\alpha = H_2, O_2$ and H_2O in the following manner:

$$C_{Cs} = 0.1[0.4 + \text{erfc}(0.1Ka_L)]^{-3.0}; a_3 = 0.48Le_\alpha^{-0.26}[0.325 + \text{erfc}(0.2Ka_L^{1.7})]^{0.4} \tag{5iii}$$

where $Ka_L = \tilde{\varepsilon}^{0.5} \delta_{th}^{0.5} S_L^{-1.5}$ is the local Karlovitz number. The predictions of the CC model with the model parameters given by Eq. 5iii are henceforth referred to as the CC-M model in this paper. It can be seen from Fig. 5 that the predictions of CC-M model show better agreement with DNS data than the TDH and CC models and this improvement is especially evident in case C where the CC-M still does not capture the correct behaviour for $\tilde{c}_T < 0.5$.

It is worth noting that the TDH model was originally proposed for non-reacting flows using the gradient hypothesis, and thus does not include the effects of flame normal acceleration due to chemical heat release and therefore is not equipped to predict the counter-gradient behaviour. The effects of heat release remain significant even for case C in spite of large values of Ka and thus, it is perhaps not surprising that this model does not perform satisfactorily for all species in all cases considered here. This behaviour has been found to be consistent with previous analyses based on simple chemistry DNS results [24, 27, 39]. This implies that the choices of species and chemical mechanism do not have significant influence on the agreement of the TDH model with $\overline{\rho u''_1 u''_1 Y''_\alpha}$ extracted from DNS data.

The functional form of the second term on the right hand side of Eq. 5ii is derived based on a presumed bi-modal distribution of Y_α with peaks at $Y_{\alpha a}$ and $Y_{\alpha b}$, which is strictly valid for $Da > 1$ and $Ka < 1$. Thus, the CC model works relatively satisfactorily for case A (where $Da > 1$ and $Ka < 1$) but the probability density function of Y_α does not remain bimodal for $Ka > 1$ and thus its performance worsens progressively with increasing Ka (i.e. from case B to case C). Some recent analyses [51, 52] focussed on modelling of the PDF of c where non bi-modal distribution is realised.

4.5 Modelling of the pressure gradient terms (T_4+T_5)

The variations of the normalised values of $(T_4 + T_5)$ with \tilde{c}_T in cases A-C are shown in Fig. 6 for $\alpha = H_2, O_2$ and H_2O . It can be seen from Fig. 6 that the net contribution of

Table 2 Optimum values of C_{Cs} and a_3 for the CC model (5ii)

	H ₂	H ₂ O	O ₂
Case A	$C_{Cs} = 0.1; a_3 = 0.6$	$C_{Cs} = 0.1; a_3 = 0.5$	$C_{Cs} = 0.1; a_3 = 0.45$
Case B	$C_{Cs} = 0.22; a_3 = 0.5$	$C_{Cs} = 0.22; a_3 = 0.4$	$C_{Cs} = 0.22; a_3 = 0.35$
Case C	$C_{Cs} = 2.7; a_3 = 0.4$	$C_{Cs} = 2.7; a_3 = 0.35$	$C_{Cs} = 2.7; a_3 = 0.3$

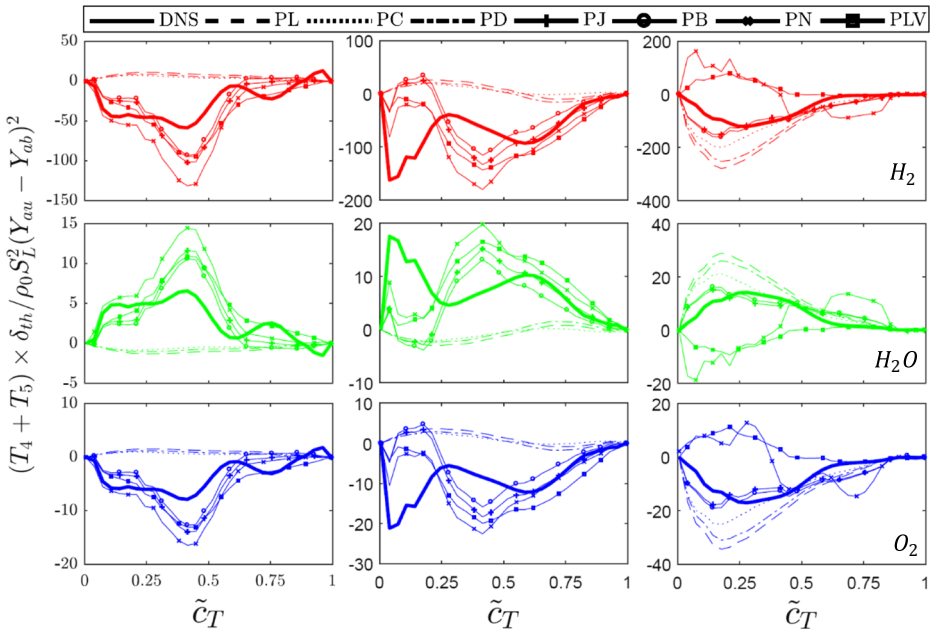


Fig. 6 Variation of $(T_4 + T_5) \times \delta_{th} / \rho_0 S_L^2 (Y_{au} - Y_{ab})^2$ with \tilde{c}_T across the flame brush along with the different model predictions for cases A-C (1st to 3rd column) for $\alpha = H_2, H_2O$ and O_2 (1st to 3rd row)

$(T_4 + T_5)$ assumes mostly negative values for the major reactants such as $\alpha = H_2$ and O_2 in all cases, whereas $(T_4 + T_5)$ exhibits positive values for $\alpha = H_2O$. The flame normal acceleration sets up a negative mean pressure gradient $\partial \bar{P} / \partial x_1$ in the statistically planar flames. According to BML analysis, one obtains: $\bar{Y}''_{\alpha} = -\bar{\rho} (Y_{au} - \tilde{Y}_{\alpha}) (\tilde{Y}_{\alpha} - Y_{ab}) \tau / \rho_0 (Y_{au} - Y_{ab})$ [9] and even though this expression is not strictly valid for $Da < 1$ it can still be used in a qualitative sense. As $Y_{au} > Y_{ab}$ ($Y_{au} < Y_{ab}$) for reactants (products) and $(Y_{au} - \tilde{Y}_{\alpha}) (\tilde{Y}_{\alpha} - Y_{ab})$ is positive semi-definite (i.e. $(Y_{au} - \tilde{Y}_{\alpha}) (\tilde{Y}_{\alpha} - Y_{ab}) \geq 0$), the quantity \bar{Y}''_{α} assumes negative (positive) values for reactants (products). Chakraborty and Cant [24] proposed $\bar{Y}''_{\alpha} = -\bar{\rho} \tilde{Y}_{\alpha}''^2 \tau / \rho_0 (Y_{au} - Y_{ab})$ for both $Da > 1$ and $Da < 1$ combustion, and this expression remains valid for all cases considered here for $\alpha = H_2, O_2$ and H_2O . Thus, the negative (positive) values of \bar{Y}''_{α} for the major reactant (product) species lead to negative (positive) values of $T_4 = -\bar{Y}''_{\alpha} (\partial \bar{P} / \partial x_1)$ (see Fig. 4). A comparison between Figs. 4 and 6 reveals that although the fluctuating pressure gradient term T_5 locally assumes values with a different sign to that of T_4 , the net contribution of $(T_4 + T_5)$ follows the sign of the mean pressure gradient term T_4 .

The mean and fluctuating pressure gradient terms are often modelled together because of their similar origin [2]. Several models are available in the existing literature for $(T_4 + T_5)$ (see Refs. [23, 27, 39]). Some of the models for $(T_4 + T_5)$, which were originally proposed for non-reacting flows, take the following form [2]:

$$T_4 + T_5 = -C_{1c} \frac{\tilde{\varepsilon}}{\bar{k}} \overline{\rho u_i'' Y_{\alpha}''} + C_{2c} \overline{\rho u_k'' Y_{\alpha}''} \frac{\partial \tilde{u}_i}{\partial x_k} + C_{3c} \overline{\rho u_k'' Y_{\alpha}''} \frac{\partial \tilde{u}_k}{\partial x_i} + C_{4c} \overline{\rho u_i'' u_k''} \frac{\partial \tilde{Y}_{\alpha}}{\partial x_k} \quad (6)$$

where C_{1c}, C_{2c}, C_{3c} and C_{4c} are the model parameters. Launder [35] suggested that $C_{1c} = 3.0, C_{2c} = 0, C_{3c} = 0$ and $C_{4c} = 0.4$, and this model will henceforth be referred to

as the PL model. Craft [36] adopted a similar model (referred to as the PC model) with $C_{1c} = 3.0, C_{2c} = 0.5, C_{3c} = 0$ and $C_{4c} = 0$. An alternative model (PD model) was suggested by Durbin [37] where $C_{1c} = 2.5, C_{2c} = 0, C_{3c} = 0$ and $C_{4c} = 0.45$. Jones [53] and Bradley et al. [54] modelled $(T_4 + T_5)$ in the following manner:

$$T_4 + T_5 = -\overline{Y''_\alpha} \frac{\partial \overline{P}}{\partial x_i} - C_{\phi 1} \frac{\tilde{\varepsilon}}{\overline{k}} \overline{\rho u''_i Y''_\alpha} + C_{\phi 2} \overline{\rho u''_k Y''_\alpha} \frac{\partial \tilde{u}_i}{\partial x_k} \tag{7}$$

where $C_{\phi 1} = 3.0$ and $C_{\phi 2} = 0.5$ are taken for the model by Jones [53] (PJ model), whereas $C_{\phi 1} = 3.0$ and $C_{\phi 2} = 0$ are considered for the model by Bradley et al. [54] (PB model). Lindstedt and Vaos [31] proposed another alternative model (PLV model) as:

$$T_4 + T_5 = -\overline{Y''_\alpha} \frac{\partial \overline{P}}{\partial x_i} + \overline{\rho u''_l Y''_\alpha} G_{il} + C_{As} \overline{Y''_\alpha} \frac{\partial \overline{P}}{\partial x_i} \tag{8}$$

where $C_{As} = 1/3$ and G_{il} is the generalised Langevin coefficient which is a function of Reynolds stress $\overline{\rho u''_i u''_j}$ and the mean velocity gradient $\partial \tilde{u}_i / \partial x_j$ [31]. It is worth noting that $\overline{Y''_\alpha}$ was evaluated using the BML relation: $\overline{Y''_\alpha} = -\overline{\rho}(Y_{\alpha u} - \tilde{Y}_\alpha)(\tilde{Y}_\alpha - Y_{\alpha b})\tau / \rho_0(Y_{\alpha u} - Y_{\alpha b})$ in Refs. [31, 54, 55] but for the current *a-priori* analysis $\overline{Y''_\alpha}$ is extracted from DNS data. In all cases considered here, $\overline{Y''_\alpha}$ can be modelled as: $\overline{Y''_\alpha} = -\overline{\rho} \tilde{Y}_\alpha'^2 \tau / \rho_0(Y_{\alpha u} - Y_{\alpha b})$ (not shown here).

Nishiki et al. [20] also proposed a model (PN model) based on *a-priori* simple chemistry DNS analysis for flames in the corrugated flamelets regime in the following manner:

$$T_4 + T_5 = C_D \frac{\overline{\rho}(Y_{\alpha u} - \tilde{Y}_\alpha)(\tilde{Y}_\alpha - Y_{\alpha b})\tau}{\rho_0(Y_{\alpha u} - Y_{\alpha b})} \frac{\partial \overline{P}}{\partial x_i} - C_{E1} \frac{\tilde{\varepsilon}}{\overline{k}} \overline{\rho u''_i Y''_\alpha} + C_{E2} \tau . S_L \overline{\omega}_{Y_\alpha} \left(1 - \frac{Y_{\alpha u} - \tilde{Y}_\alpha}{Y_{\alpha u} - Y_{\alpha b}} \right)^{1.7} \tag{9}$$

where $C_D = 0.8, C_{E1} = 0.38$ and $C_{E2} = 0.66$ are the model constants. The first term on the right hand side of the PN model originates from the BML relation for T_4 [9].

The predictions of all the aforementioned models are compared to $(T_4 + T_5)$ extracted from DNS data in Fig. 6 for $\alpha = H_2, O_2$ and H_2O . Figure 6 shows that the PL, PC and PD models fail to capture both qualitative and quantitative behaviours of $(T_4 + T_5)$ in cases A and B irrespective of the choice of α . By contrast, these models predict the qualitative behaviour of $(T_4 + T_5)$ satisfactorily in case C. These models overpredict the magnitude of $(T_4 + T_5)$ towards the unburned gas side of the flame brush, whereas quantitative agreement with DNS data remains reasonable towards the burned gas side of the flame brush. The PL, PC and PD models were originally proposed for incompressible non-reacting flows [2, 34–36] where the contribution of $T_4 = -\overline{Y''_\alpha} \partial \overline{P} / \partial x_i$ is identically zero and thus its contribution was ignored. It can be seen from Fig. 4 that the contribution of T_4 remains significant for the cases considered here irrespective of the choice of α . A comparison of cases A–C in Fig. 4 shows that the contribution of T_4 in comparison to T_5 diminishes from case A to case C, and thus the PL, PC and PD models are found to be more successful in capturing the statistical behaviour of $(T_4 + T_5)$ in case C. The case C belongs to the broken reaction zones regime and thus it shows some attributes of non-reacting flows, which is also reflected in the more satisfactory performance of the PL, PC and PD models than in cases A and B.

The PJ, PB and PLV models exhibit very similar behaviour. All three models capture the qualitative behaviour of (T_4+T_5) in case A for $\alpha=H_2, O_2$ and H_2O , but these models underpredict (overpredict) the magnitude of (T_4+T_5) towards the unburned (burned) gas side of the flame brush. In case B, these models fail to predict the behaviour of (T_4+T_5) on the unburned gas side of the flame brush, but capture both quantitative and the qualitative behaviours on the burned gas side of the flame brush. The PJ and PB models perform satisfactorily in case C for $\alpha=H_2, O_2$ and H_2O but the PLV model does not capture the qualitative and quantitative behaviours of (T_4+T_5) in this case for all the major species considered here.

The PN model captures the qualitative behaviour of (T_4+T_5) better than the other alternative models in case A but overpredicts the magnitude. In case B, the PN model captures the qualitative behaviour, but underpredicts the magnitude on the unburned gas side and overpredicts the magnitude on the burned gas side of the flame brush. However, in case C, the PN model fails to predict the qualitative behaviour and the magnitude of (T_4+T_5) on the unburned gas side, whereas it accurately captures the behaviour on the burned gas side of the flame brush but overpredicts the magnitude of (T_4+T_5) . The PN model was originally proposed for strict flamelet combustion (i.e. $Da > 1$ and $Ka < 1$) and these assumptions are rendered invalid for the broken reaction zones regime in case C and thus this model does not perform satisfactorily in this case for all species considered here.

It is worth noting that the PL, PC, PD models, which do not account for the leading order contribution of $T_4 = -\bar{Y}''_\alpha \partial \bar{P} / \partial x_i$, are not successful in capturing (T_4+T_5) extracted from DNS data. However, the PJ, PB and PN models, which include $T_4 = -\bar{Y}''_\alpha \partial \bar{P} / \partial x_i$ are more successful in capturing the behaviour of $(T_4 + T_5)$ extracted from DNS data than the PL, PC, PD models. The model parameter and the model expression for the PLV model have been calibrated for the flamelet regime of combustion and thus it is perhaps unsurprising that this model does not perform satisfactorily in case C representing the broken reaction zones regime. The first term on the right hand side of the PN model (9) assumes a bi-modal distribution of c , which is not realised in cases B and C and thus the prediction of the PN model exhibits some inaccuracies especially in these cases. It is possible that the methodologies, which parameterise the pdf of c when the presumed bi-modal pdf with impulses at $c = 0$ and $c = 1.0$ is not realised, can be more successful in deriving improved models for (T_4+T_5) for non-flamelet regime of combustion.

4.6 Modelling of the molecular diffusion terms (T_6+T_7)

The variations of normalised $(T_6 + T_7)$ with \tilde{c}_T in cases A-C are shown in Fig. 7 for $\alpha = H_2, O_2$ and H_2O . It can be seen from a comparison between Figs. 2 and 7 that $(T_6 + T_7)$ assumes a sign which is opposite to $\overline{\rho u_1'' Y_\alpha''}$ for all species α in all cases. These terms tend to oppose the dominant behaviour of the turbulent scalar flux $\overline{\rho u_1'' Y_\alpha''}$. In cases A and B, $(T_6 + T_7)$ assumes positive (negative) values for $\alpha = H_2$ and O_2 ($\alpha = H_2O$), whereas $\overline{\rho u_1'' Y_\alpha''}$ exhibits negative (positive) values throughout the flame brush [9, 12, 24, 27, 39]. By contrast, in case C, $(T_6 + T_7)$ assumes negative (positive) values for $\alpha = H_2$ and O_2 ($\alpha = H_2O$), whereas $\overline{\rho u_1'' Y_\alpha''}$ exhibits a positive (negative) value throughout the flame brush.

According to Bray et al. [9] $(T_6 + T_7)$ is modelled as:

$$(T_6 + T_7) = K_1 \frac{\overline{\rho u_1'' Y_\alpha''}}{\bar{\rho}(Y_{\alpha u} - \tilde{Y}_\alpha)} \frac{\overline{\omega \dot{Y}_\alpha}(Y_{\alpha u} - Y_{\alpha b})}{(\tilde{Y}_\alpha - Y_{\alpha b})} \tag{10}$$

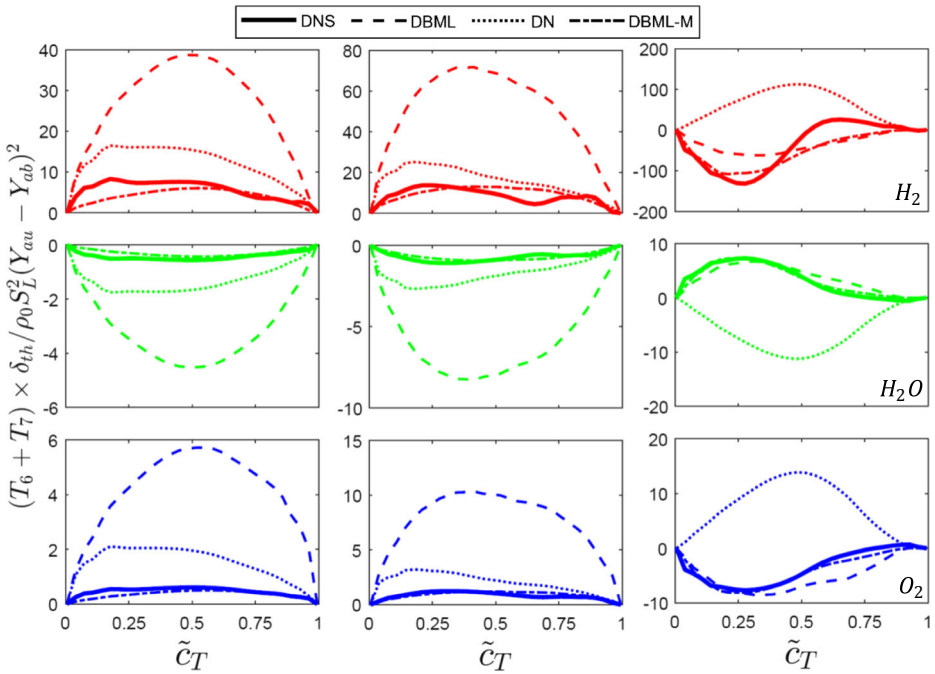


Fig. 7 Variation of $(T_6 + T_7) \times \delta_{th} / \rho_0 S_L^2 (Y_{au} - Y_{ab})^2$ with \tilde{c}_T across the flame brush along with the different model predictions for cases A-C (1st to 3rd column) for $\alpha = H_2, H_2O$ and O_2

where $\overline{\omega_{Y_\alpha}}$ is the chemical reaction rate of α , and $K_1 = 0.85$ is the model constant. The model given by Eq. 10 will henceforth be referred to as the DBML model. An alternative model (i.e. DN model) was proposed by Nishiki et al. [20] in the following manner:

$$(T_6 + T_7) = -C_F \tau S_L \overline{\omega_{Y_\alpha}} \tag{11}$$

where $C_F = 0.4$ is a model constant. It is worthwhile to note that both Eqs. 10 and 11 are directly proportional to the mean reaction rate $\overline{\omega_{Y_\alpha}}$ and thus these models predict non-zero values of $(T_6 + T_7)$ within the flame brush.

The predictions of the DBML, DN and DC models are compared to $(T_6 + T_7)$ extracted from DNS data in Fig. 7. It can be seen from Fig. 7 that both DBML and DN models satisfactorily capture the qualitative behaviours of $(T_6 + T_7)$ for $\alpha = H_2, O_2$ and H_2O . However, both DBML and DN models overpredict the magnitudes of $(T_6 + T_7)$ in cases A and B but the extent of overprediction is relatively smaller in the case of the DN model.

The DBML analysis was originally proposed for the strict flamelet regime (i.e. $Da > 1$ and $Ka < 1$) but even then this model significantly overpredicts $(T_6 + T_7)$ in case A where the conditions in terms of Da and Ka for which the model was proposed are satisfied (using $K_1 = 0.2$ instead of 0.85 provides satisfactory quantitative agreement with DNS data). The same can be said for the DN model where $C_F = 0.2$ instead of 0.4 yields good quantitative agreement with DNS data. Thus, the application of these models for case C (where $Da < 1$ and > 1) is beyond the scope of their validity. In spite of the above limitation, the DBML model predicts the correct sign of $(T_6 + T_7)$ for $\alpha = H_2, O_2$ and H_2O in case C and the

quantitative agreement with DNS data also remains reasonable. The choice of characteristic dissipation time-scale $K_1 \overline{\omega_{\tilde{Y}_\alpha}} (Y_{\alpha u} - Y_{\alpha b}) / [\overline{\rho} (Y_{\alpha u} - \tilde{Y}_\alpha) (\tilde{Y}_\alpha - Y_{\alpha b})]$ in the DBML model may not be appropriate for low-Damköhler number (i.e. $Da < 1$) combustion in case C and this might be one of the reasons behind the overprediction of the DBML model in this case. The DN model is strictly valid only for counter-gradient transport and it predicts wrong sign for gradient transport [24, 27, 39]. Thus, the DN model fails to predict the correct qualitative behaviour of $(T_6 + T_7)$ for $\alpha = H_2, O_2$ and H_2O in case C where a gradient transport is obtained (see Fig. 4).

The optimum values of K_1 for different cases for $\alpha = H_2, O_2$ and H_2O are listed in Table 3. As the DN model cannot predict the correct sign in the case of gradient transport, the optimum values C_F for cases A-C have not been reported in Table 3. It can be seen that the optimum K_1 values for cases A-C are different. Moreover, optimum values of K_1 for $\alpha = H_2$ are different from the corresponding optimum values for $\alpha = O_2$ and H_2O . Furthermore, optimum values of K_1 are similar for $\alpha = O_2$ and H_2O . The Lewis number of H_2 is significantly smaller than unity (i.e. $Le_{H_2} \ll 1$), whereas the Lewis numbers for $\alpha = O_2$ and H_2O (i.e. Le_{O_2} and Le_{H_2O}) are close to unity. Thus, the variations of the optimum values of K_1 in Table 3 suggests that it is likely to be dependent on Karlovitz and Lewis numbers. Based on this, the optimum value of K_1 has been parameterised as:

$$K_1 = 0.1 Le_\alpha^{-0.5} [0.3 + erf c(0.1 Ka_L)]^{-2} \tag{12}$$

According to this parameterisation, K_1 reaches an asymptotic for large values of Ka_L . The predictions of the DBML model with K_1 according to Eq. 12 (i.e. DBML-M model) are shown in Fig. 7, which shows that Eq. 12 significantly improves the model performance and the DBML-M model satisfactorily captures both qualitative and quantitative behaviours of $(T_6 + T_7)$. It is worth noting that Eq. 12 provides a possible parameterisation of K_1 and an alternative parameterisation exhibiting similar behaviour is also possible.

4.7 Modelling of the reaction rate term T_8

The reaction rate contribution to the turbulent scalar flux transport was modelled by Bray et al. [9] for strict flamelet combustion (i.e. $Da > 1$ and $Ka < 1$) in the following manner (i.e. RB model):

$$T_8 = -C_R \left[\phi_m - \frac{Y_{\alpha u} - \tilde{Y}_\alpha}{Y_{\alpha u} - Y_{\alpha b}} \right] \overline{\omega_{\tilde{Y}_\alpha}} \frac{\overline{\rho u'' Y_\alpha''}}{\rho Y_\alpha''^2} (Y_{\alpha u} - Y_{\alpha b}) \tag{13}$$

where $C_R = 1.0$ and $\phi_m = 0.5$ are the model constants. The variations of normalised T_8 with \tilde{c}_T for cases A-C are shown in Fig. 8 for $\alpha = H_2, O_2$ and H_2O along with the predictions of the RB model. Figure 8 shows that in cases A and B, the term T_8 assumes negative values towards the unburned gas side and positive values on the burned gas side of the flame

Table 3 Optimum value of K_1 for the DBML model (10)

	H ₂	H ₂ O	O ₂
Case A	0.175	0.1	0.1
Case B	0.2	0.125	0.125
Case C	1.5	0.9	0.85

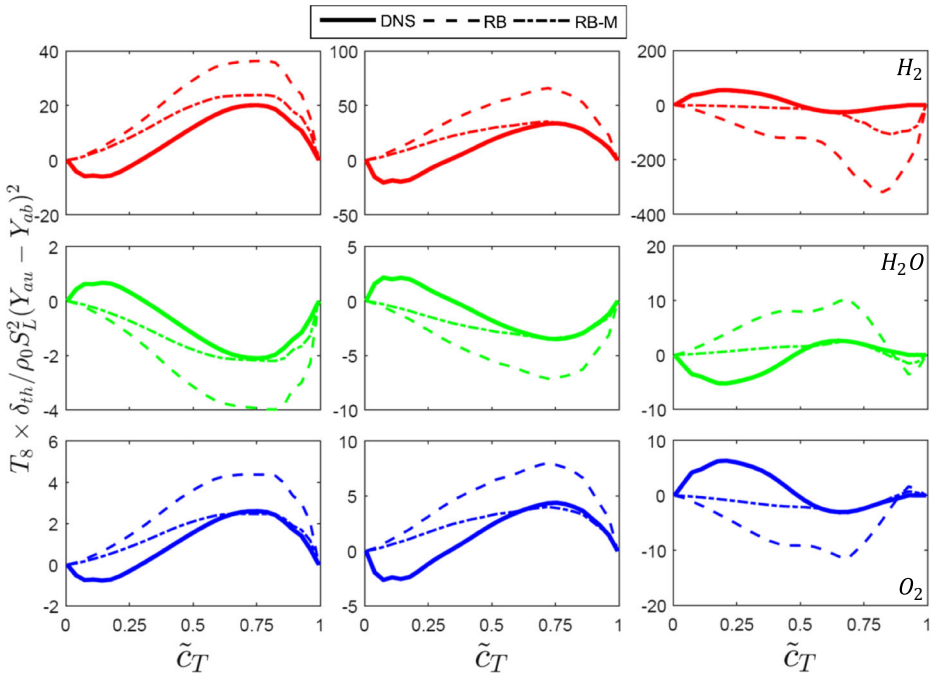


Fig. 8 Variation of $T_8 \times \delta_{th} / \rho_0 S_L^2 (Y_{au} - Y_{ab})^2$ with \tilde{c}_T across the flame brush along with the different model predictions for cases A-C (1st to 3rd column) for $\alpha = H_2, H_2O$ and O_2

brush for $\alpha = H_2$ and O_2 , whereas just the opposite behaviour is observed for $\alpha = H_2O$. By contrast, in case C, T_8 assumes positive (negative) values towards the unburned gas side and negative (positive) values on the burned gas side of the flame brush for $\alpha = H_2$ and O_2 ($\alpha = H_2O$). This implies that the correlation between the fluctuations of velocity and reaction rate is fundamentally different in case C than in cases A and B. In the case of counter-gradient transport, a positive fluctuation of velocity induced by an increase in reaction rate magnitude tends to produce negative (positive) values of T_8 for reactant (product) species such as H_2 and O_2 (H_2O) and this is predominantly responsible for the observed behaviours of T_8 towards the unburned gas side and middle of the flame brush in cases A and B. However, the reaction rate magnitude tends to decrease towards the burned gas side whereas temperature continues to rise which acts to increase the positive fluctuations of velocity due to thermal expansion in the case of predominant counter-gradient transport. This leads to negative (positive) values of T_8 for reactant (product) species such as H_2 and O_2 (H_2O) and this is predominantly responsible for the observed behaviours of T_8 towards the burned gas side of the flame brush in cases A and B. Due to a predominantly gradient transport in case C, an increase in reaction rate magnitude tends to induce negative fluctuations of velocity, which leads to positive (negative) values of T_8 for reactant (product) species such as H_2 and O_2 (H_2O) towards the unburned gas side and middle of the flame brush. In case C, the reaction rate magnitude tends to decrease towards the burned gas side whereas the rising temperature acts to decrease velocity due to augmented viscous damping, which is reflected in the negative (positive) values on the burned gas side of the flame brush for $\alpha = H_2$ and O_2 ($\alpha = H_2O$).

Table 4 Optimum value of C_R for the RB model (13)

	H ₂	H ₂ O	O ₂
Case A	0.90	0.525	0.60
Case B	0.65	0.475	0.55
Case C	0.10	0.175	0.225

It can be seen from Fig. 8 that the RB model captures the correct qualitative behaviour of T_8 for $\alpha = H_2$, O_2 and H_2O in cases A and B. Although the quantitative agreement of the RB model with DNS data is not perfect, it is reasonable for these cases and this level of agreement has been found to be consistent with previous findings based on simple chemistry DNS data [24, 27, 39]. The qualitative and quantitative agreement between the RB model and DNS data is comparatively less satisfactory in case C in comparison to cases A and B. It is worth noting that the RB model was originally proposed for $Da > 1$ and $Ka < 1$, and thus the performance of this model progressively worsens with increasing (decreasing) Ka (Da).

It has been found that the performance of the RB model is not significantly dependent on ϕ_m but on C_R . The optimum values of C_R for different cases for $\alpha = H_2$, O_2 and H_2O are listed in Table 4, which shows that C_R decreases from case A to case C and its value is different for different species. Moreover, optimum values of C_R for $\alpha = H_2$ are greater than the corresponding optimum values for $\alpha = O_2$ and H_2O . The optimum values of C_R for $\alpha = O_2$ and H_2O are similar in magnitude. Thus, it can be inferred that the optimum values of C_R is dependent on Karlovitz and Lewis numbers, which can be parameterised as:

$$C_R = 0.17Le_\alpha^{-1.0}[Le_\alpha + \text{erfc}(0.1Ka_L)]^2 \quad (14)$$

The predictions of the RB model with $\phi_m = 0.5$ and C_R according to Eq. 14 (i.e. RB-M model) are also shown in Fig. 8, which shows that Eq. 14 significantly improves the model performance and the RB-M model satisfactorily captures both qualitative and quantitative behaviours of T_8 . It is worth noting that Eq. 14 provides a possible parameterisation of C_R and an alternative parameterisation exhibiting similar behaviour is also possible.

4.8 Final Remarks on the Turbulent Scalar Flux Transport Equation

A summary of the models considered for this analysis is presented in Table 5. Based on the foregoing discussion, the optimal combinations of the closure models for the unclosed terms of the turbulent scalar flux transport equation for different combustion regimes for different species (e.g. Eqs. 5iii, 12 and 14 are dependent on Le_α) are summarised in Table 6 for the convenience of readers and future users of the turbulent scalar flux transport equation. Table 6 provides an idea about the appropriate models for major species in different combustion regimes. It can be appreciated from the information provided in Table 6 that there is a huge scope for improvement in the modelling of the turbulent scalar flux transport in the broken reaction zones regime and this aspect needs further investigation. Further, it becomes clear that for most unclosed terms there is not a single existing model that performs satisfactorily in all regimes of combustion and for all species (see Tables 2–4). The suggested empirical relations accounting for some of these effects for CC, DBML and RB models will require further investigation.

Table 5 Summary of optimal models for different combustion regimes for $\alpha = H_2, O_2$ and H_2O

Term	Model	Model Expression
$\overline{\rho u_j'' u_i'' Y_\alpha''}$	TDH	$\overline{\rho u_j'' u_i'' Y_\alpha''} = -C_{CS} \frac{\bar{k}}{\bar{\rho}} \overline{\rho u_j'' u_k'' \frac{\partial(\overline{\rho u_i'' Y_\alpha'' / \bar{P}})}{\partial x_k}}, C_{CS} = 0.22$
	CC	$\overline{\rho u_1'' u_1'' Y_\alpha''} = -C_{CS} \frac{\bar{k}}{\bar{\rho}} \overline{\rho u_1'' u_1'' \frac{\partial(\overline{\rho u_1'' Y_\alpha'' / \bar{P}})}{\partial x_1}} - \frac{\bar{P}(Y_{\alpha u} - \bar{Y}_\alpha)(\bar{Y}_\alpha - Y_{\alpha b})}{(Y_{\alpha u} - Y_{\alpha b})}$
	CC-M	$\left[1 - 2\sqrt{g} \frac{Y_{\alpha u} - \bar{Y}_\alpha}{(Y_{\alpha u} - Y_{\alpha b})} \right] \left[\frac{-\overline{\rho u_1'' Y_\alpha'' (Y_{\alpha u} - Y_{\alpha b})}}{\bar{P}(Y_{\alpha u} - \bar{Y}_\alpha)(\bar{Y}_\alpha - Y_{\alpha b})} + a_3 \sqrt{\frac{\overline{\rho u_1'' u_1''}}{\bar{P}}} \right]^2$ where $g = \frac{\overline{\rho Y_\alpha''^2}}{\bar{P}(Y_{\alpha u} - \bar{Y}_\alpha)(\bar{Y}_\alpha - Y_{\alpha b})}$ $C_{CS} = 0.22, a_3 = 0.5$ (for CC model) $C_{CS} = 0.1[0.4 + \text{erfc}(0.1Ka_L)]^{-3.0}$ (for CC-M model) $a_3 = 0.48Le_\alpha^{-0.26}[0.325 + \text{erfc}(0.2Ka_L^{1.7})]^{0.4}$ (for CC-M model)
$T_4 + T_5$		$T_4 + T_5 = -C_{1c} \frac{\bar{k}}{\bar{\rho}} \overline{\rho u_i'' Y_\alpha''} + C_{2c} \overline{\rho u_k'' Y_\alpha'' \frac{\partial \bar{u}_i}{\partial x_k}} + C_{3c} \overline{\rho u_k'' Y_\alpha'' \frac{\partial \bar{u}_k}{\partial x_i}} + C_{4c} \overline{\rho u_i'' u_k'' \frac{\partial \bar{Y}_\alpha}{\partial x_k}}$
	PL	$C_{1c} = 3.0, C_{2c} = 0, C_{3c} = 0$ and $C_{4c} = 0.4$
	PC	$C_{1c} = 3.0, C_{2c} = 0.5, C_{3c} = 0$ and $C_{4c} = 0$
	PD	$C_{1c} = 2.5, C_{2c} = 0, C_{3c} = 0$ and $C_{4c} = 0.45$
	PJ	$T_4 + T_5 = -\bar{Y}_\alpha'' \frac{\partial \bar{P}}{\partial x_i} - C_{\phi 1} \frac{\bar{k}}{\bar{\rho}} \overline{\rho u_i'' Y_\alpha''} + C_{\phi 2} \overline{\rho u_k'' Y_\alpha'' \frac{\partial \bar{u}_i}{\partial x_k}}$ $C_{\phi 1} = 3.0$ and $C_{\phi 2} = 0.5$
	PB	$C_{\phi 1} = 3.0$ and $C_{\phi 2} = 0$
	PLV	$T_4 + T_5 = -\bar{Y}_\alpha'' \frac{\partial \bar{P}}{\partial x_i} + \overline{\rho u_l'' Y_\alpha'' G_{il}} + C_{As} \bar{Y}_\alpha'' \frac{\partial \bar{P}}{\partial x_i}$, $C_{As} = 1/3$ and G_{il} is the generalised Langevin coefficient
	PN	$T_4 + T_5 = C_D \frac{\bar{P}(Y_{\alpha u} - \bar{Y}_\alpha)(\bar{Y}_\alpha - Y_{\alpha b})\tau}{\rho_0(Y_{\alpha u} - Y_{\alpha b})} \frac{\partial \bar{P}}{\partial x_i} - C_{E1} \frac{\bar{k}}{\bar{\rho}} \overline{\rho u_i'' Y_\alpha''}$ $+ C_{E2} \tau \cdot S_L \bar{\omega}_{Y_\alpha} \left(1 - \frac{Y_{\alpha u} - \bar{Y}_\alpha}{Y_{\alpha u} - Y_{\alpha b}} \right)^{1.7}, C_D = 0.8, C_{E1} = 0.38$ and $C_{E2} = 0.66$
$T_6 + T_7$	DBML	$(T_6 + T_7) = K_1 \overline{\rho u_1'' Y_\alpha'' \frac{\omega_{Y_\alpha} (Y_{\alpha u} - Y_{\alpha b})}{\bar{P}(Y_{\alpha u} - \bar{Y}_\alpha)(\bar{Y}_\alpha - Y_{\alpha b})}}$
	DBML-M	$K_1 = 0.85$ (for DBML model) $K_1 = 0.1Le_\alpha^{-0.5}[0.3 + \text{erfc}(0.1Ka_L)]^{-2}$ (for DBML-M model)
	DN	$(T_6 + T_7) = -C_F \tau S_L \bar{\omega}_{Y_\alpha}, C_F = 0.4$
T_8	RB	$T_8 = -C_R \left[\phi_m - \frac{Y_{\alpha u} - \bar{Y}_\alpha}{Y_{\alpha u} - Y_{\alpha b}} \right] \bar{\omega}_{Y_\alpha} \frac{\overline{\rho u_1'' Y_\alpha''}}{\rho Y_\alpha''^2} (Y_{\alpha u} - Y_{\alpha b})$
	RB-M	$C_R = 1.0$ and $\phi_m = 0.5$ (for RB model) $C_R = 0.17Le_\alpha^{-1.0}[Le_\alpha + \text{erfc}(0.1Ka_L)]^2$ and $\phi_m = 0.5$ (for RB-M model)

Table 6 Summary of optimal models for different combustion regimes for $\alpha = H_2, O_2$ and H_2O . CF, TRZ and BRZ refer to the corrugated flamelets, thin reaction zones and broken reaction zones regimes, respectively

	CF (Case A)			TRZ (Case B)			BRZ (Case C)		
	H_2	H_2O	O_2	H_2	H_2O	O_2	H_2	H_2O	O_2
$\overline{\rho u_j'' u_i'' Y_\alpha''}$	CC-M	CC-M	CC-M	CC-M	CC-M	CC-M	CC-M	CC-M	CC-M
$T_4 + T_5$	PLV	PLV	PLV	PN	PN	PN	PB	PB	PB
$T_6 + T_7$	DBML-M	DBML-M	DBML-M	DBML-M	DBML-M	DBML-M	DBML-M	DBML-M	DBML-M
T_8	RB-M	RB-M	RB-M	RB-M	RB-M	RB-M	RB-M	RB-M	RB-M

5 Conclusions

The statistical behaviours of the turbulent scalar flux and the terms of its transport equation for major species have been analysed in the context of RANS using a detailed chemistry DNS database of freely-propagating H_2 –air flames with an equivalence ratio of 0.7 spanning the corrugated flamelets, thin reaction zones and broken reaction zones regimes of combustion. The turbulent scalar flux statistics and its transport have been analysed in detail for the major reactants and products (i.e. H_2 , O_2 and H_2O). A counter-gradient transport has been observed for the cases considered here representing the corrugated flamelets and thin reaction zones regimes of combustion, whereas a gradient transport is observed for the case representing the broken reaction zones regime. Accordingly, the qualitative behaviours of the terms of the turbulent scalar flux transport equation remain similar for the flames representing the corrugated flamelets and thin reaction zones regimes but these behaviours are different to that observed for the broken reaction zones regime flame considered here. It has been found that the performances of the existing closures for turbulent transport, pressure gradient, molecular diffusion and reaction rate terms show some dependence on the choice of the major species. The models for the unclosed terms of the turbulent scalar flux transport equation which perform satisfactorily in the corrugated flamelets and thin reaction zones regimes of premixed combustion have been identified based on *a-priori* DNS analysis. However, there is no existing modelling methodology which was originally developed for the broken reaction zones combustion and thus the existing closures for the unclosed terms of the turbulent scalar flux transport equation, which were originally proposed for the strict flamelet combustion, have been found to be mostly inadequate for the broken reaction zones regime. Detailed explanations have been provided for the observed performances of sub-models for the unclosed terms of the turbulent scalar flux transport equation for different regimes of premixed turbulent combustion. The present analysis indicates that there is ample scope for improvement in the modelling of the unclosed terms in the turbulent scalar flux transport equation and this improvement is especially needed for the broken reaction zone regime combustion.

Acknowledgements The financial and computational support of EPSRC and ARCHER are gratefully acknowledged.

Funding Information This study was funded by EPSRC (EP/K025163/1).

Compliance with Ethical Standards

Conflict of interests The authors declare that they have no conflict of interest.

Open Access This article is distributed under the terms of the Creative Commons Attribution 4.0 International License (<http://creativecommons.org/licenses/by/4.0/>), which permits unrestricted use, distribution, and reproduction in any medium, provided you give appropriate credit to the original author(s) and the source, provide a link to the Creative Commons license, and indicate if changes were made.

Publisher's Note Springer Nature remains neutral with regard to jurisdictional claims in published maps and institutional affiliations.

References

1. Launder, B.E.: Heat and mass transport by turbulence. *Top. Appl. Phys.* **12**, 231–287 (1976)
2. Durbin, P.A., Pettersson-Reif, B.A.: *Statistical Theory and Modelling for Turbulent Flows*. Wiley (2001)
3. Kim, J., Moin, P.: Transport of passive scalars in a turbulent channel flow. *Turb. Shear Flows* **6**, 85–95 (1989)
4. Abe, K., Suga, K.: Towards the development of a Reynolds-averaged of algebraic scalar flux model. *Int. J. Heat Fluid Flow* **22**, 19–29 (2001)
5. Guo, Y., Xu, C., Cui, G., Zhang, Z.: Large eddy simulation of scalar turbulence using a new subgrid Eddy diffusivity model. *Int. J. Heat Fluid Flow* **28**, 268–274 (2007)
6. Murman, S.M.: A scalar anisotropy model for turbulent eddy viscosity. *Int. J. Heat Fluid Flow* **42**, 115–130 (2013)
7. Rossi, R., Philips, D.A., Iaccarino, G.: A numerical study of scalar dispersion downstream of a wall-mounted using direct simulations and algebraic closures. *Int. J. Heat Fluid Flow* **31**, 805–819 (2010)
8. van Hooff, T., Blocken, B., Glousseau, P., van Heijst, G.J.F.: Counter-gradient diffusion in a slot-ventilated enclosure assessed by LES and RANS. *Comput. Fluids* **96**, 63–75 (2014)
9. Bray, K.N.C., Libby, P.A., Moss, J.B.: Unified modelling approach for premixed turbulent combustion – Part I: General formulation. *Combust. Flame* **61**, 87–102 (1985)
10. Cheng, R.K., Shepherd, I.G.: Influence of burner geometry on premixed turbulent flame propagation. *Combust. Flame* **85**, 7–26 (1991)
11. Rutland, C.J., Cant, R.S.: Turbulent transport in premixed flames. In: *Proc. of 1994 Summer Program, Centre for Turbulence Research Stanford University/NASA Ames* (1994)
12. Veynante, D., Trouvé, A., Bray, K.N.C., Mantel, T.: Gradient and counter-gradient turbulent scalar transport in turbulent premixed flames. *J. Fluid Mech.* **332**, 263–293 (1997)
13. Veynante, D., Poinso, T.: Effects of pressure gradient in turbulent premixed flames. *J. Fluid Mech.* **353**, 83–114 (1997)
14. Boger, M.: *Sub-Grid Scale Modeling for Large Eddy Simulation of Turbulent Premixed Combustion*. PhD dissertation, E' cole Centrale Paris (2000)
15. Swaminathan, N., Bilger, R.W., Cuenot, B.: Relationship between turbulent scalar flux and conditional dilatation in premixed flames with complex chemistry. *Combust. Flame* **126**, 1764–1779 (2001)
16. Rymer, G.: *Analysis and Modelling of the Mean Reaction Rate and Transport Terms in Turbulent Premixed Combustion*. PhD dissertation, E' cole Centrale Paris (2001)
17. Kalt, P.A.M., Chen, Y.C., Bilger, R.W.: Experimental investigation of turbulent scalar flux in premixed stagnation-type flames. *Combust. Flame* **129**, 401–415 (2002)
18. Tullis, S.W., Cant, R.S.: Scalar transport modelling in large Eddy simulation of turbulent premixed flames. *Proc. Combust. Inst.* **29**, 2097–2104 (2003)
19. Huai, Y., Sadiki, A., Pfadler, S., Löffler, M., Beyrau, F., Leipertz, A., Dinkelacker, F.: Experimental assessment of scalar flux models for large eddy simulations of reacting flows. *Turb. Heat Mass Transfer* **5**, 263–266 (2006)
20. Nishiki, S., Hasegawa, T., Borghi, R., Himeno, R.: Modelling of turbulent scalar flux in turbulent premixed flames based on DNS database. *Combust. Theory Modell.* **10**, 39–55 (2006)
21. Richard, S., Colin, O., Vermorel, O., Angelberger, C., Benkenida, A., Veynante, D.: Large eddy simulation of combustion in spark ignition engine. *Proc. Combust. Inst.* **31**, 3059–3066 (2007)
22. Pfadler, S., Kerl, J., Beyrau, F., Leipertz, A., Sadiki, A., Scheuerlein, J., Dinkelacker, F.: Direct evaluation of the subgrid-scale scalar flux in turbulent premixed flames with conditioned dual-plane stereo PIV. *Proc. Combust. Inst.* **32**, 1723–1730 (2009)
23. Chakraborty, N., Cant, R.S.: Effects of Lewis number on scalar transport in turbulent premixed flames. *Phys. Fluids* **21**, 035110.1 (2009)
24. Chakraborty, N., Cant, R.S.: Effects of Lewis number on turbulent scalar transport and its modelling in turbulent premixed flames. *Combust. Flame* **156**, 1427–1444 (2009)
25. Chakraborty, N., Cant, R.S.: Physical insight and modelling for Lewis number effects on turbulent heat and mass transport in turbulent premixed flames. *Num. Heat Trans.* **55**, 762–779 (2009)
26. Lecocq, G., Richard, S., Colin, O., Vervisch, L.: Gradient and counter-gradient modelling in premixed flames: Theoretical study and application to the LES of a Lean premixed turbulent swirl-burner. *Combust. Sci. Technol.* **182**, 465–479 (2010)
27. Chakraborty, N., Cant, R.S.: Effects of turbulent Reynolds number on the modelling of turbulent scalar flux in premixed flames. *Numer. Heat Trans. A* **67**(12), 1187–1207 (2015)
28. Gao, Y., Chakraborty, N., Klein, M.: Assessment of sub-grid scalar flux modelling in premixed flames for large Eddy simulations: A-priori direct numerical simulation. *Eur. J. Mech. Fluids-B* **52**, 97–108 (2015)

29. Gao, Y., Chakraborty, N., Klein, M.: Assessment of the performances of sub-grid scalar flux models for premixed flames with different global Lewis numbers: A direct numerical simulation analysis. *Int. J. Heat Fluid Flow* **52**, 28–39 (2015)
30. Klein, M., Chakraborty, N., Gao, Y.: Scale similarity based models and their application to subgrid scale scalar flux modelling in the context of turbulent premixed flames. *Int. J. Heat Fluid Flow* **57**, 91–108 (2016)
31. Lindstedt, R.P., Vaos, E.M.: Modelling of premixed turbulent flames with second moment methods. *Combust. Flame* **116**, 461–485 (1999)
32. Tian, L., Lindstedt, R.P.: The impact of dilatation, scrambling, and pressure transport in turbulent premixed flames. *Combust. Theor. Modell.* **21**, 1114–1147 (2017)
33. Lindstedt, R.P.: Transported Probability Density Function Methods for Turbulent Premixed Flames with Second Moment Methods in Turbulent Premixed Flames, pp. 102–130. Cambridge University Press (2011)
34. Daly, B.J., Harlow, F.H.: Transport equations of turbulence. *Phys. Fluids* **13**, 2634–2649 (1970)
35. Launder, B.L.: Second-moment closure: present and future. *Int. J. Heat Fluid Flow* **10**, 282–300 (1989)
36. Craft, T., Graham, L., Launder, B.: Impinging jet studies for turbulence model assessment –II. An examination of the performance of four turbulence models. *Int. J. Heat Mass Transfer* **36**, 2687–2697 (1993)
37. Durbin, P.A.: A Reynolds stress model for near-wall turbulence. *J. Fluid Mech.* **249**, 465–493 (1993)
38. Peters, N.: *Turbulent Combustion*. 1st edn. Cambridge University Press, Cambridge (2000)
39. Lai, J., Alwazzan, D., Chakraborty, N.: Turbulent scalar flux transport in head-on quenching of turbulent premixed flames: A direct numerical simulations approach to assess models for Reynolds averaged Navier Stokes simulations. *J. Turbul.* **18**, 1033–1066 (2017)
40. Li, S.C., Kong, Y.H.: Diesel combustion modelling using les turbulence model with detailed chemistry. *Combust. Theor. Model* **12**, 208–219 (2008)
41. Vermorel, O., Richard, S., Colin, O., Angelberger, C., Benkenida, A., Veynante, D.: Towards the understanding of cyclic variability in a spark ignited engine using multicycle LES. *Combust. Flame* **156**, 1525–1541 (2009)
42. Im, H.G., Chen, J.H.: Preferential diffusion effects on the burning rate of interacting turbulent premixed hydrogen-air flames. *Combust. Flame* **126**, 246–258 (2002)
43. Arias, P.G., Chaudhuri, S., Uranakara, H.A., Im, H.G.: Direct numerical simulations of statistically stationary turbulent premixed flame. *Combust. Sci. Technol.* **188**, 1182–1198 (2016)
44. Yoo, C.S., Wang, Y., Trounev, A., Im, H.G.: Characteristic boundary conditions for direct simulations of turbulent counterflow flames. *Combust. Theor. Modell.* **9**, 617–646 (2005)
45. Rogallo, R.S.: Numerical Experiments in Homogeneous Turbulence. NASA TM81315. NASA Ames Research Center, California (1981)
46. Passot, T., Pouquet, A.: Compressible Turbulence with a perfect gas law: A numerical. Approach. *J. Fluid Mech.* **181**, 441–466 (1987)
47. Han, K.Y.: Roles of displacement speed on evolution of flame surface density for different turbulent intensities and Lewis numbers in turbulent premixed combustion. *Combust. Flame* **152**, 194–205 (2008)
48. Reddy, H., Abraham, J.: Two-dimensional direct numerical simulation evaluation of the flame-surface density model for flames developing from an ignition kernel in lean methane/air mixtures under engine conditions. *Phys. Fluids* **24**, 105–108 (2012)
49. Dopazo, C., Cifuentes, L., Martin, J., Jimenez, C.: Strain rates normal to approaching iso-scalar surfaces in a turbulent premixed flame. *Combust. Flame* **162**, 1729–1736 (2015)
50. Wacks, D.H., Chakraborty, N., Klein, M., Arias, P.G., Im, H.G.: Flow topologies in different regimes of premixed turbulent combustion: A direct numerical simulation analysis. *Phys. Rev. Fluids* **1**, 083401 (2016)
51. Salehi, M.M., Bushe, W.K., Shahabzian, N., Groth, C.P.T.: Modified laminar flamelet presumed probability density function for LES of premixed turbulent combustion. *Proc. Combust. Inst.* **34**, 1203–1211 (2013)
52. Mura, A., Robin, V., Kha, K.Q.N., Champion, M.: A layered description of a premixed flame stabilized in stagnating turbulence. *Combust. Sci. Technol.* **188**, 1592–1602 (2016)
53. Jones, W.P.: Turbulence modelling and numerical solution methods for variable density and combusting flows. In: Libby, P.A., Williams, F.A. (eds.) *Turbulent Reacting Flows*, pp. 309–374. Academic Press, London (1994)
54. Bradley, D., Gaskell, P.H., Gu, X.J.: Application of a Reynolds stress, stretched flamelet, mathematical model to computations to turbulent burning velocities and comparison with experiments. *Combust. Flame* **96**, 221–248 (1994)
55. Domingo, P., Bray, K.N.C.: Laminar flamelet expressions for pressure fluctuation terms in second moment models of premixed turbulent combustion. *Combust. Flame* **121**, 555–574 (2000)

Affiliations

V. Papapostolou¹ · N. Chakraborty¹ · M. Klein² · H. G. Im³

V. Papapostolou
v.s.papapostolou1@newcastle.ac.uk

M. Klein
markus.klein@unibw.de

H. G. Im
hong.im@kaust.edu.sa

¹ School of Engineering, Newcastle University, Newcastle-Upon-Tyne, NE17RU, UK

² Department of Aerospace Engineering, Bundeswehr University Munich, Werner-Heisenberg-Weg 39, 85577 Neubiberg, Germany

³ Clean Combustion Research Center, King Abdullah University of Science and Technology (KAUST), Thuwal 23955-6900, Saudi Arabia